.

Formation and annihilation of E4 centers in ZnO: Influence of hydrogen

A. Hupfer, C. Bhoodoo, L. Vines, and B. G. Svensson

Citation: J. Appl. Phys. **119**, 181506 (2016); doi: 10.1063/1.4948241
View online: http://dx.doi.org/10.1063/1.4948241
View Table of Contents: http://aip.scitation.org/toc/jap/119/18
Published by the American Institute of Physics

AIP | Journal of Applied Physics
INTRODUCING INVITED PERSPECTIVES
Ultrafast magnetism and THz spintronics
Authors: Jakob Walowski and Markus Münzenberg

RIGHTSLINK

JOURNAL OF APPLIED PHYSICS **119**, 181506 (2016)

Formation and annihilation of E4 centers in ZnO: Influence of hydrogen

A. Hupfer, C. Bhoodoo, L. Vines, and B. G. Svensson
Physics Department/Centre for Materials Science and Nanotechnology, University of Oslo, P.O. Box 1048, Blindern, Oslo N-0316, Norway

(Received 17 November 2015; accepted 3 February 2016; published online 5 May 2016)

Hydrothermally grown n-type ZnO bulk samples have been implanted with protons and deuterium ions to fluences in the range of 8×10^{10} to $8 \times 10^{11}\,\mathrm{cm}^{-2}$. The implantations were performed at the temperature of 285 K, and the samples were then analyzed *in-situ* by deep level transient spectroscopy (DLTS) using a setup connected to the implanter beam line. The concentration of the so-called E4 center, having an apparent energy level at ~0.57 eV below the conduction edge, is found to increase linearly with the ion fluence and the generation rate is proportional to the elastic energy deposition, as expected for a primary defect. Isothermal annealing of the E4 center at temperatures between 290 and 315 K reveals first-order kinetics with the activation energy of ~0.6 eV. The annealing rate is strongly enhanced with increasing hydrogen fluence, and a model invoking migration of interstitial hydrogen and subsequent reaction with E4 exhibits close agreement with the experimental data. The rate of electron capture by E4 during the DLTS filling pulse depends on temperature, and it displays a thermal barrier of ~0.15 eV. Most of these experimental results for E4 conform to the theoretically predicted properties of the oxygen vacancy (V_O) and a tentative assignment of E4 to V_O is made, corroborating previous suggestions in the literature. In particular, the 0.57 eV level is ascribed to the double donor state of V_O. *Published by AIP Publishing.*
[http://dx.doi.org/10.1063/1.4948241]

I. INTRODUCTION

Zinc oxide (ZnO) is a wide bandgap semiconductor ($E_g \approx 3.4$ eV) that has received considerable attention in the past few years and is presently used in many diverse products, notably piezoelectric transducers, varistors, and transparent conductive films. While classical semiconductor applications, such as photovoltaics and UV-light emitting diodes and lasers, are certainly attractive for ZnO, it has also been proposed as a host material for spintronics and quantum computing due to its low spin-orbit coupling.[1] In most of these applications, point defects play an important role.[2] For instance, a prerequisite for spintronic devices is a fundamental understanding of deep level defects serving as a base for spin-manipulations with a very weak coupling to the environment.

Two prominent electrically active point defects detected in n-type ZnO material are the so-called E3-center and E4-center with energy level positions ~0.30 eV and ~0.57 eV below the conduction band edge, E_c, respectively.[3] The E3-center occurs in all types of ZnO materials, irrespective of the growth method used, but exhibits no (or weak) response on irradiation by MeV electrons, protons, and self-ions.[4,5] However, recently Hupfer *et al.*[6] showed that the E3 concentration is drastically enhanced by hydrogen implantation and unambiguous evidence for the involvement of hydrogen in the E3 center was put forward. The E4 center, on the other hand, exhibits usually much lower concentrations than E3 in as-grown material but increases considerably with the irradiation/implantation fluence of electrons, protons, and heavier ions.[3,5] Further, both Frank *et al.*[7] and Ellguth *et al.*[8] reported a negative-U behavior of the E4 center, albeit with different positions of the energy levels involved, and several authors have tentatively assigned it to the oxygen vacancy (V_O).[7,9] Moreover, E4 is strongly promoted by annealing in Zn-rich ambient and suppressed by annealing in O-rich ambient in a reversible manner, and Quemener *et al.*[9] deduced a formation energy of ~1.9 eV under Zn-rich conditions.

As discussed in Ref. 10, the generation rate of the E4 center extracted from the results for the MeV proton and helium irradiated samples by Auret *et al.*[3] is low and only on the order of ~0.2%–0.3% of the total vacancy (or interstitial) generation. These irradiations were performed at room temperature (RT), and Vines *et al.*[4] have found that E4 starts to disappear already at post-implant annealing temperatures below 400 K. This implies a low thermal stability of the irradiation-induced E4 centers and/or a high probability to react with other defects mobile at RT (or just above). In the present study, we have undertaken implantation by 325 keV protons and deuterium ions, allowing monitoring of the whole implantation-induced defect versus depth-distribution by deep level transient spectroscopy (DLTS) at sample temperatures below RT. Moreover, the sample analysis was performed on-line, i.e., the DLTS setup used was connected to the implanter beam line enabling *in-situ* analysis immediately after the implantation without exposing the samples to RT. Accordingly, thermally activated defect migration is suppressed, and indeed, the E4 concentration is found to increase strongly with the ion fluence. The presence of hydrogen is shown to drastically enhance the E4 annealing rate during post-implant heat treatment at temperatures around RT. Our results corroborate the tentative assignment of E4 to V_O made in the literature, and the rapid disappearance of E4 in the presence of hydrogen may be attributed to a reaction with interstitial hydrogen, H_i, forming the thermodynamically more stable H_O center.

RIGHTSLINK

II. EXPERIMENTAL

Wafers of hydrothermally grown n-type ZnO (HT-ZnO) purchased from Tokyo Denpa were cut into $5 \times 5\,\mathrm{mm}^2$ sized samples. The samples were cleaned in acetone and ethanol. After a 40 s treatment in boiling H_2O_2 (31%), 100 nm thick Pd Schottky contacts were deposited on the Zn-polar face using electron-beam evaporation. The Schottky contacts displayed a rectification of more than two orders of magnitude between the forward and reverse bias (+2 V and −2 V). The samples were then implanted at 285 K with 325 keV protons (H^+) or deuterium ions (D^+), having a projected range of $\approx$2.0 μm as estimated by Monte Carlo simulations using the SRIM code,[11] and fluences between 2×10^{11} and $3.5 \times 10^{11}\,\mathrm{cm}^{-2}$, and 8×10^{10} and $8 \times 10^{11}\,\mathrm{cm}^{-2}$, respectively.

The DLTS measurements were carried out *in situ* while scanning the sample temperature from 200 to 260 K using a refined version of the setup described in Ref. 12 connected to the implanter beamline. A reverse bias of −7 V was applied with a filling pulse of 7 V and 50 ms duration. The bulk net carrier concentration was determined through capacitance-voltage (CV) measurements (1 MHz probing frequency) in the scanned temperature range. For the defect concentration versus depth profiling a single rate DLTS window was applied, and the temperature was held constant within ±0.2 K at the maximum of the studied peak. The steady-state reverse bias voltage was kept constant while gradually increasing the amplitude of the filling pulse, and the depth profile was subsequently extracted from the dependence of the DLTS signal on the pulse amplitude.

III. RESULTS AND DISCUSSION

A. Formation of E4

Figure 1 shows the charge carrier concentration (N_d) versus depth, extracted from CV measurements carried out at 220 K, in samples implanted with D^+ ions. Prior to the implantation, the samples displayed an almost uniform carrier concentration of $\approx 8 \times 10^{14}\,\mathrm{cm}^{-3}$ at depths $\gtrsim$0.8 μm, while closer to the surface, an increase was observed. The calculated profile of implanted deuterium ions in Fig. 1 as obtained by SRIM simulations[11] (dashed line) corresponds to the lowest fluence used, $2 \times 10^{11}\,\mathrm{cm}^{-2}$. Fig. 1 shows that the implantation causes an increase in the charge carrier concentration which largely follows the deuterium profile. Because of this increase in N_d and the limit of the maximum applicable reverse bias voltage, the probe region becomes more shallow with fluence, and all the profiles could not be monitored to the same maximum depth. The increase in N_d is, indeed, attributed to the implanted D ions, which can not only act as shallow donors but also exhibit a strong reactivity with impurities/defects leading to passivation of acceptors.[13] In comparison to the H^+ implanted samples (results not shown), the increase in N_d in Fig. 1 is about one order of magnitude lower and also shows some dependence on the sample used. The elastic energy deposition is substantially higher for 325 keV D^+ ions than for 325 keV H^+ ions, resulting in an almost three times higher total vacancy (and interstitial) generation per ion in the former case, as estimated by SRIM simulations.[11] Hence, the presence of implantation-induced defects as well as of residual defects/impurities in the as-grown samples appear to limit the net increase in N_d by the implanted D^+ and H^+ ions. The limitation can arise from both direct passivation of generated deep acceptor-like centers and charge carrier compensation.

Figure 2 shows the DLTS spectra corresponding to the implantations in Fig. 1. Two levels are observed, labeled E3 and E4. The pronounced peak at ~160 K (E3) has an energy position of $E_c - 0.30\,\mathrm{eV}$, while E4 occurs at $E_c - 0.57\,\mathrm{eV}$. E3 is the most prominent peak in the as grown sample and is present with a concentration of $\approx$60% of N_d. We have shown previously that the E3 formation involves hydrogen and is drastically enhanced after implanting H^+ ions.[6] The same holds for D^+ ions, and E3 will not be discussed here further. Before implantation, no other defect levels could be detected in the spectra when scanning the temperature from RT down to 15 K.

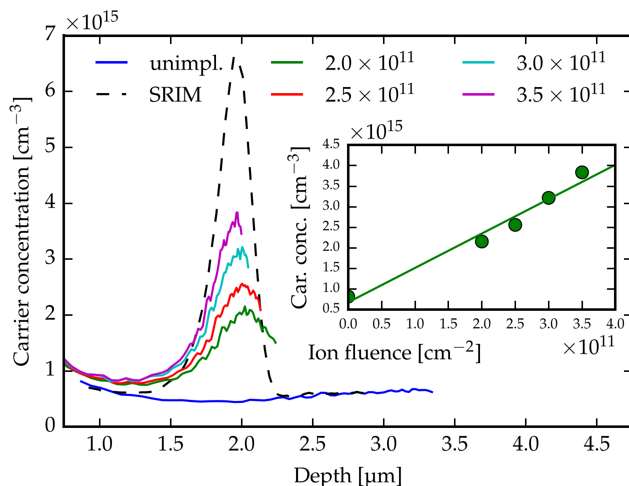

FIG. 1. Influence of deuterium fluence (per cm^2) on the charge carrier profile. Results are also shown for the sample prior to implantation. The calculated profile of implanted deuterium ions corresponds to a fluence of $2 \times 10^{11}\,\mathrm{cm}^{-2}$, and was obtained using the SRIM-code.[11] The inset shows the profile peak concentration versus ion fluence, revealing a linear dependence.

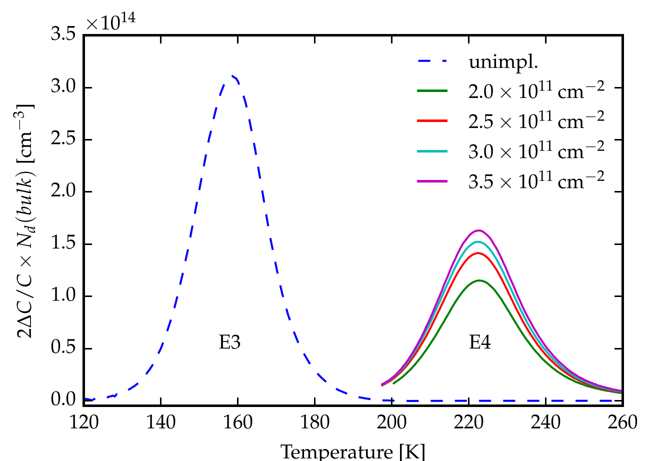

FIG. 2. DLTS spectra of samples before implantation (dashed line) and after implantation with different fluences of deuterium. Rate window = (640 ms)$^{-1}$.

RIGHTSLINK

In the implanted samples, the E4 peak amplitude increases with the D (and H) fluence, in accordance with previous reports for electron and proton irradiated samples.[3] DLTS spectra constructed by applying the high energy resolution weighting functions of GS4 and GS6-type[14] reveal only one level contribution to the E4 peak and no evidence of multiple levels is found. The E4 peak amplitude grows almost linearly with the D fluence in Fig. 2, as expected for a primary intrinsic defect, like V_O. However, it should be noted that a quantitative conversion of the DLTS peak amplitude to concentration is strictly valid for uniform defect profiles only. Thus, depth profiling measurements are highly appropriate for the studied samples, and the obtained results are shown in Fig. 3. Before implantation, no E4 centers are found while after the implantation their concentration increases with depth up to the profile peak at $\sim 2\,\mu$m and then decreases rapidly, having a shape resembling that of the simulated V_O profile. The absolute concentration of E4 grows strongly with the D-fluence, consistent with the data in Fig. 2. Similar to that for the carrier-versus-depth profiles in Fig. 1, the probing depth for E4 decreases with the D-fluence because of the concurrent increase in N_d and limited applicable maximum reverse bias voltage. The dashed profile in Fig. 3 shows V_O according to SRIM simulations assuming a displacement energy threshold of 68 eV and 43 eV for substitutional O and Zn atoms, respectively.[15] Dynamic annealing is not accounted for in the SRIM simulations whilst ZnO is generally regarded to be a radiation-hard material with pronounced dynamic annealing.[10] In monocrystalline silicon, which also exhibits strong dynamic annealing, a few percent of implantation-induced vacancies and self-interstitials are estimated to survive immediate recombination during low fluences at RT.[16] Indeed, assuming a fraction of $\sim$1% of surviving V_O's, an excellent quantitative agreement is obtained between the measured E4 profiles and the calculated V_O ones, as illustrated for the highest fluence implant in Fig. 3. The value of $\sim$1% appears quite reasonable for a primary defect in comparison with that for silicon, and the close resemblance in shape between the experimental and calculated profiles corroborates the assumption of E4 arising from a low-order (primary) defect. This is also supported by the linear dependence of the E4 profile peak concentration on the ion fluence, shown in the inset of Fig. 3 for both D^+ and H^+ ions.

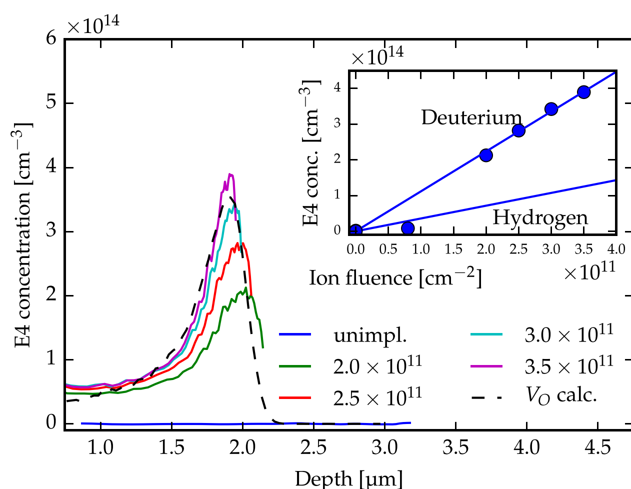

FIG. 3. Influence of deuterium fluence (per cm^2) on the E4 center concentration versus depth profile. The calculated profile of the oxygen vacancy (V_O) concentration corresponds to the highest fluence implantation and was obtained using the SRIM-code[11] by assuming a fraction of 1% the V_O's surviving dynamic annealing. The inset shows the fluence dependency of the maximum of the E4 profile after implantation. The highest fluence used for hydrogen ($8 \times 10^{11}\,\text{cm}^{-1}$) is outside the range shown but falls on the solid line drawn for the H^+ ions.

Here, it should be clearly emphasized that the arguments put forward for assigning the E4 level to V_O in conjunction with Fig. 3 are not exclusive. In principle, similar arguments can be used for any of the three other primary defects (V_{Zn}, Zn_i, and O_i), albeit with slightly different absolute values for the fraction surviving dynamic annealing. On the other hand, both V_{Zn} and O_i are deep double-acceptor centers with their charge state transitions occurring in the lower part of the energy band whilst Zn_i is a shallow donor with the level position located very close to E_c.[17,18] Thus, V_O appears as the most plausible origin of the E4 level.

B. Annealing of E4

The inset of Fig. 4 shows the evolution of the E4 concentration-versus-depth profile maximum in two hydrogen implanted samples as a function of time during isothermal annealing at 300 and 315 K. The anneals were performed at zero bias voltage. The evolution follows a single exponential decay showing a first order kinetics process, and rate constants deduced from annealing at 315, 310, 300, and 290 K obey an Arrhenius behavior (Fig. 4). The value extracted for the activation energy, E_a, is $\sim$0.6 eV with a pre-exponential factor of $\sim 2 \times 10^5\,\text{s}^{-1}$. Basically, first-order annealing kinetics of a defect center can arise from two different processes: either (i) dissociation of the center or (ii) a diffusion-limited reaction with another defect/impurity species having a concentration about one order of magnitude (or more) higher than that of the defect center itself. For (i), a pre-exponential factor on the order of $\sim 10^{13}\,\text{s}^{-1}$ is anticipated,[19] and dissociation is, therefore, ruled out as a mechanism responsible for the loss of E4.

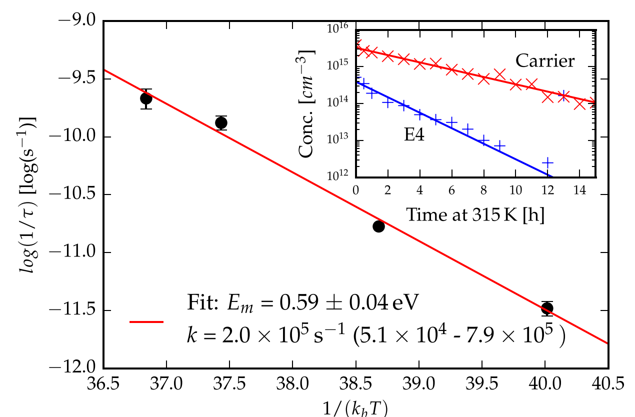

FIG. 4. Arrhenius plot for the annealing rate constants of the E4 depth profile peak concentration in the hydrogen implanted samples. Error bars are indicated and too small to be seen in some cases. The inset shows the peak concentrations of E4 and N_d as a function of annealing time at 315 K.

RIGHTSLINK

However, process (ii) appears as a likely candidate. Fig. 5 shows the E4 concentration-versus-depth profile maximum versus annealing time at 300 K for two samples implanted with a high (8×10^{11} cm^{-2}) and a low (8×10^{10} cm^{-2}) fluence of protons, respectively. The implantations were performed with an identical flux of 1×10^{10} ions/cm^2 s and between the measurements, and the samples were kept at zero bias voltage. The initial rise in the E4 trap concentration in the high fluence sample for durations $\lesssim$1 h is artificial and stems from that the maximum of applicable reverse bias was not sufficient to monitor the whole implanted region when the net carrier concentration remained above $\sim 4 \times 10^{15}$ cm^{-3}.

A striking feature of the data in Fig. 5 is that the E4 annealing rate increases strongly with the H$^+$ fluence. This implies an involvement of hydrogen in the annealing process with migration of interstitial hydrogen, H_i, as a likely ingredient. H_i is known to be rather mobile already at RT[20,21] and assuming the reaction $H_i + E4 \rightarrow HE4$, the following rate equation can be derived for the loss of E4 by applying the theory for diffusion-limited reactions:[22,23]

$$\frac{d[E4]}{dt} = -4\pi R D_{H_i}[H_i][E4], \tag{1}$$

where square brackets denote concentration, t is the annealing time, R is the capture radius for the reaction, and D_{H_i} the diffusivity of H_i. Since $[H_i] \gg [E4]_{t=0}$, the solution of Eq. (1) reduces to $[E4] = [E4]_{t=0}e^{-ct}$ with the annealing rate constant c being

$$c = 4\pi R D_{H_i}[H_i] = 4\pi R D_{H_{i0}}[H_i]e^{-E_m(H_i)/kT}, \tag{2}$$

where $E_m(H_i)$ represents the migration energy of H_i and $D_{H_{i0}}$ is the pre-exponential factor of D_{H_i}.

Thus, the experimentally determined E_a value of $\sim$0.6 eV (Fig. 4) can be associated with $E_m(H_i)$, consistent with previous reports in the literature yielding values of $E_m(H_i)$ in the range of $\sim$0.5–0.9 eV.[20,21] Further, putting $[H_i]$ equal the carrier concentration immediately after the implantation, $N_d(t = 0)$, i.e., prior to when a deep acceptor-like center starts to evolve and reduce the net carrier concentration,[24]

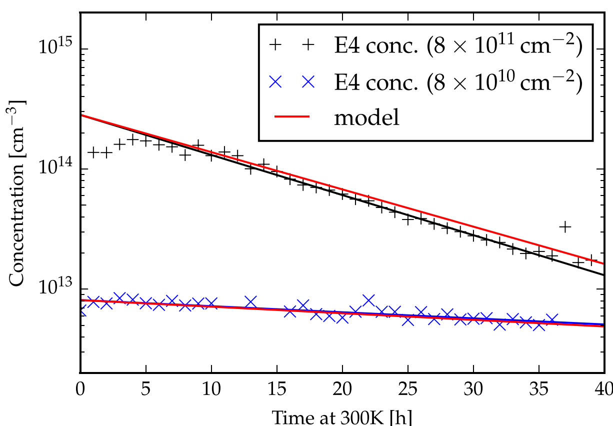

FIG. 5. Time evolution of the E4 depth profile peak concentration (x) for a sample implanted with a high (8×10^{11} cm^{-2}) (black) or low (8×10^{10} cm^{-2}) H$^+$ fluence (blue).

one obtains $RD_{H_{i0}} = 1.4 \times 10^{-11}$ cm^3 s^{-1} by equaling the pre-exponential factor in Eq. (2) to the measured value of $\sim 2 \times 10^5$ s^{-1}. Assuming $R = 5$ Å, based on geometrical considerations and omitting possible electrostatic interactions, $D_{H_{i0}}$ becomes equal to $\sim 3 \times 10^{-4}$ cm^2 s^{-1}, which is close to that anticipated for a typical interstitial migration process.[25] A direct comparison between the experimental and modeled values for the decay of [E4] is given in Fig. 5, and the agreement is excellent. In particular, the experimental annealing rate constant scales approximately linearly with the H fluence, in full accordance with Eq. (2) of the model.

As discussed in Section III A, V_O is a probable candidate for the identity of E4, which is also corroborated by the E4 annealing results presented in this section. Hydrogenation of V_O via reaction with H_i is very likely leading to the formation of the thermodynamically more stable H_O configuration ($H_i + V_O \rightarrow H_O$), as predicted by Janotti and Van de Walle.[26]

C. Charge state transitions of V_O and the E4 level

Theoretically, overwhelming evidence exists for V_O being a negative-U double donor center,[27–29] i.e., the energy position of the (+/0) transition lies below that of the (2+/+) transition. Experimentally, Frank *et al.*[7] and especially Ellguth *et al.*[8] have presented firm evidence for a negative-U behavior of the E4 center. A negative-U behavior is typically associated with large lattice relaxations of the defect such that the resulting energy gain overcomes the Coulomb repulsion of the two electrons, leading to a net attractive electron interaction. Two prominent examples of negative-U centers are the mono-vacancy in silicon[30] and the carbon vacancy in silicon carbide.[31] Indeed, the V_O center is predicted to exhibit large lattice relaxations with the four Zn nearest neighbor atoms displaced inward by $\sim$12% for V_O^0 and outward by $\sim$2% and 23% for V_O^+ and V_O^{2+}, respectively.[32] Most of the recent results based on density functional theory (DFT), predominantly obtained using hybrid functionals combined with different correction schemes, yield a position of $\sim E_C - 1.0$ eV for the thermodynamic (2+/0) V_O transition with a negative-U value of $\sim$1.0 eV.[33] This places the (+/0) and (2+/+) transitions at $\sim$1.5 eV and $\sim$0.5 eV below E_c, respectively. However, it should be underlined that a large scatter exists between the theoretical estimates where some authors in early studies have placed the (2+/0) transition $\sim$0.2 eV above the valence band edge.[34]

Because of the negative-U character, the V_O^+ configuration is not stable in thermodynamic equilibrium, but it can play a decisive role at non-equilibrium conditions such as those encountered in DLTS measurements. Assuming that the V_O donor states are located in the upper part of the bandgap, V_O is doubly positively charged in the space charge region during the DLTS stage of quiescent reverse bias while during the filling pulse stage it captures one electron and becomes singly positively charged. As commonly found for defects with strong lattice coupling,[35] the electron capture is likely to occur via a multi-phonon process enabling the surmounting of a possible energy barrier for changing from the V_O^{2+} configuration to the V_O^+ one, see *EB1* in the schematic

RIGHTSLINK Copyright Clearance Center

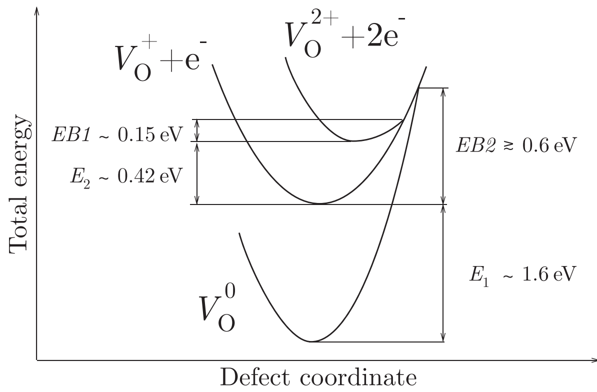

FIG. 6. Schematic configuration coordinate diagram for the oxygen vacancy (V_O) and its charge states. Thermal barrier energies (*EB1* and *EB2*) and electronic transition energies (E_1 and E_2) derived from experimental data of E4 are indicated.

configuration coordinate diagram composed in Fig. 6. Subsequently, one more electron can be captured via a similar process leading to the $V_O^+ \rightarrow V_O^0$ transformation, provided that the filling pulse duration is sufficient and the configuration energy barrier is small (*EB2* in Fig. 6).

Fig. 7 displays the E4 peak amplitude as a function of the filling pulse duration at sample temperatures between 210 and 245 K. The rate of the capture process reveals a clear increase with the temperature, shifting the filling curves to shorter pulse lengths. In the inset of Fig. 7, the filling pulse durations at half of the full peak amplitude are given versus the reciprocal thermal energy. The values exhibit an Arrhenius behavior and the capture is thermally activated with an energy of ~0.15 eV.

In the DLTS study by Frank *et al.*,[7] the E4 level was ascribed to the (+/0) transition of V_O by a comparison with theoretical work of Van de Walle.[36] However, this comparison is confusing; Fig. 1 in Ref. 36 shows clearly that the theory predicts a position of $\sim E_C - 1.3$ eV for the V_O (+/0) transition, i.e., much deeper than the E4 position and also in accordance with more recent DFT results.[28] Ellguth *et al.*[8] conducted a comprehensive study of point defects in ZnO thin films using a variant of optical DLTS (ODLTS) where

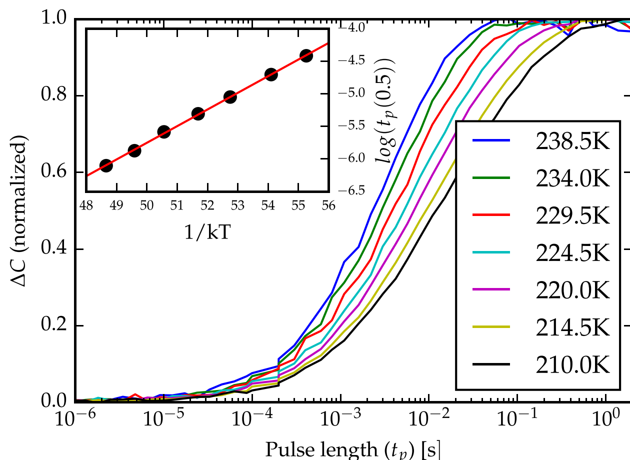

FIG. 7. Normalized ΔC as a function of bias pulse length t_p. The logarithm of the 50% value of t_p shows an Arrhenius behavior with an activation energy of 0.15 eV.

electrical pulses were used for trap filling and monochromatic light to excite carriers from the traps. Especially, strong evidence was obtained for E4 being a double donor center where an electron from the deeper-lying state, labelled $E4_2$, could be excited to the conduction band irrespective of whether the shallow state, labelled $E4_1$, is occupied or not. This property is consistent with a negative-U center but not with a positive-U one. The positions of $E4_1$ and $E4_2$ were found to be ~0.55 eV and ~1.6 eV below E_C, respectively. Furthermore, the E4 peak amplitude in ordinary DLTS measurements was found to double during additional illumination with photons having energies above ~1.7 eV, corroborating the double donor character of E4.

On the basis of the experimental results in Ref. 8 and those in Fig. 7, the configuration coordinate diagram composed in Fig. 6 can be used for interpretation of the E4 data, assuming that E4 is due to V_O. The measured barrier of ~0.15 eV for the electron capture by E4 is assigned to *EB1*, i.e., the thermal energy barrier for the $V_O^{2+} \rightarrow V_O^+$ transformation, and accordingly, the E4 level (and the $E4_1$ ODLTS level) arise from the V_O (2+/+) transition. Further, $E4_2$ is ascribed to the V_O (+/0) transition where the thermal barrier *EB2* for the $V_O^+ \rightarrow V_O^0$ electron capture is so high ($\gtrsim$0.6 eV) that the rate of capture becomes smaller than the rate of electron emission from V_O^+ to E_C during the DLTS measurements. In fact, the assignments made in Fig. 6 based on the experimental data for E4 are in good agreement with the positions of the thermodynamic charge state transitions of V_O usually predicted by DFT-calculations.[28] However, it seems that the calculated configuration coordinate diagram for V_O^0, V_O^+, and V_O^{2+} in Ref. 28 underestimates the thermal energy barriers for the $V_O^{2+} \rightarrow V_O^+$ and $V_O^+ \rightarrow V_O^0$ transformations by ~0.15 eV and ~0.3 eV, respectively, but gives the same relative trend ($EB2 > EB1$).

D. Conclusion

Both the net carrier concentration and the E4 concentration in the bulk n-type HT-ZnO samples are found to increase linearly with the fluence of H^+ and D^+ ions implanted at 285 K. The E4 generation rate is proportional to the elastic energy deposition with a ratio of ~1% relative to the rate of ballistically generated V_O defects, evidencing strong dynamic defect annealing in ZnO.

Hydrogen is shown to enhance the rate of loss of the E4 concentration during post-implant annealing and a model assuming migration of H_i with subsequent trapping by E4 (H_i + E4 → HE4) gives excellent agreement with the experimental data. The annealing process has a thermal activation energy of ~0.6 eV which is ascribed to H_i migration. These data support an assignment of E4 to V_O where H_i reacts with V_O to form the more thermodynamically stable H_O configuration.

The process of electron capture by E4 exhibits a thermal barrier of ~0.15 eV which is associated with a barrier for transforming from the V_O^{2+} configuration to the V_O^+ one. Moreover, this implies that (2+/+) thermodynamic transition of V_O occurs at $\sim E_C - 0.4$ eV, in close agreement with that usually predicted by results from DFT-based calculations.[36] However, it appears that DFT results underestimate the

RIGHTSLINK

thermal energy barriers for the $V_O^{2+} \rightarrow V_O^{+}$ and $V_O^{+} \rightarrow V_O^{0}$ transformations by $\sim$0.15 and $\gtrsim$0.3 eV, respectively, but give the same trend as indicated by the experimental data ($EB2 > EB1$).

ACKNOWLEDGMENTS

This work was supported by the Norwegian Research Council through the FriPro Program (WEDD Project) and the Norwegian Micro- and Nano-Fabrication Facility NorFab (197411/V30). We also acknowledge access to high-performance computing resources at USIT/UiO through the Norwegian Metacenter for Computational Science (NOTUR).

[1]J. R. Weber, W. F. Koehl, J. B. Varley, A. Janotti, B. B. Buckley, C. G. Van de Walle, and D. D. Awschalom, PNAS **107**, 8513 (2010).
[2]F. Tuomisto and I. Makkonen, Rev. Mod. Phys. **85**, 1583 (2013).
[3]F. D. Auret, S. A. Goodman, M. Hayes, M. J. Legodi, H. A. van Laarhoven, and D. C. Look, Appl. Phys. Lett. **79**, 3074 (2001).
[4]L. Vines, J. Wong-Leung, C. Jagadish, E. V. Monakhov, and B. G. Svensson, Phys. B: Phys. Condens. Matter **407**, 1481 (2012).
[5]L. Vines, J. Wong-Leung, C. Jagadish, V. Quemener, E. V. Monakhov, and B. G. Svensson, Appl. Phys. Lett. **100**, 212106 (2012).
[6]A. Hupfer, C. Bhoodoo, L. Vines, and B. G. Svensson, Appl. Phys. Lett. **104**, 092111 (2014).
[7]T. Frank, G. Pensl, R. Tena-Zaera, J. Zúñiga-Pérez, C. Martínez-Tomás, V. Muñoz-Sanjosé, T. Ohshima, H. Itoh, D. Hofmann, D. Pfisterer, J. Sann, and B. Meyer, Appl. Phys. A **88**, 141 (2007).
[8]M. Ellguth, M. Schmidt, R. Pickenhain, H. von Wenckstern, and M. Grundmann, Phys. Status Solidi (B) **248**, 941 (2011).
[9]V. Quemener, L. Vines, E. V. Monakhov, and B. G. Svensson, Appl. Phys. Lett. **100**, 112108 (2012).
[10]E. V. Monakhov, A. Y. Kuznetsov, and B. G. Svensson, J. Phys. D: Appl. Phys. **42**, 153001 (2009).
[11]J. F. Ziegler, M. D. Ziegler, and J. P. Biersack, Nucl. Instrum. Method B **268**, 1818 (2010).
[12]B. G. Svensson, K. H. Rydén, and B. M. S. Lewerentz, J. Appl. Phys. **66**, 1699 (1989).
[13]C. G. Van de Walle, Phys. Rev. Lett. **85**, 1012 (2000).
[14]A. A. Istratov, J. Appl. Phys. **82**, 2965 (1997).
[15]K. E. Knutsen, A. Galeckas, A. Zubiaga, F. Tuomisto, G. C. Farlow, B. G. Svensson, and A. Y. Kuznetsov, Phys. Rev. B **86**, 121203 (2012).
[16]B. G. Svensson, C. Jagadish, A. Hallén, and J. Lalita, Phys. Rev. B **55**, 10498 (1997).
[17]A. Janotti and C. G. Van de Walle, Phys. Rev. B **76**, 165202 (2007).
[18]F. Oba, A. Togo, and I. Tanaka, Phys. Rev. B **77**, 245202 (2008).
[19]J. W. Corbett, *Electron Radiation Damage in Semiconductors and Metals*, edited by F. Seitz and D. Turnbull (Academic Press, New York, 1966).
[20]K. M. Johansen, J. S. Christensen, E. V. Monakhov, A. Y. Kuznetsov, and B. G. Svensson, Appl. Phys. Lett. **93**, 152109 (2008).
[21]M. Wardle, J. Goss, and P. Briddon, Phys. Rev. Lett. **96**, 205504 (2006).
[22]T. R. Waite, Phys. Rev. B **107**, 463 (1957).
[23]T. R. Waite, J. Chem. Phys. **28**, 103 (1958).
[24]C. Bhoodoo, A. Hupfer, L. Vines, and B. G. Svensson, "Evolution kinetics of elementary point defects in ZnO implanted with low fluences of helium at cryogenic temperature" (to be published).
[25]P. M. Fahey, P. B. Griffin, and J. D. Plummer, Rev. Mod. Phys. **61**, 289 (1989).
[26]A. Janotti and C. G. Van de Walle, Nat. Mater. **6**, 44 (2007).
[27]S. B. Zhang, S. H. Wei, and A. Zunger, Phys. Rev. B **63**, 075205 (2001).
[28]A. Janotti and C. G. Van de Walle, Appl. Phys. Lett. **87**, 122102 (2005).
[29]D. M. Hofmann, D. Pfisterer, J. Sann, B. K. Meyer, R. Tena-Zaera, V. Munoz-Sanjose, T. Frank, and G. Pensl, Appl. Phys. A **88**, 147 (2007).
[30]G. D. Watkins, in MRS Proceedings, edited by J. Narayan and T. Y. Tan (Mater. Res. Soc. Proc., 1980), Vol. 2, p. 21.
[31]N. T. Son, X. T. Trinh, L. S. Løvlie, B. G. Svensson, K. Kawahara, J. Suda, T. Kimoto, T. Umeda, J. Isoya, T. Makino, T. Ohshima, and E. Janzén, Phys. Rev. Lett. **109**, 187603 (2012).
[32]A. Janotti and C. G. Van de Walle, Rep. Prog. Phys. **72**, 126501 (2009).
[33]A. Alkauskas, P. Deák, J. Neugebauer, A. Pasquarello, and C. G. Van de Walle, *Advanced Calculations for Defects in Materials: Electronic Structure Methods* (Wiley-VCH, 2011).
[34]A. F. Kohan, G. Ceder, D. Morgan, and C. G. Van de Walle, Phys. Rev. B **61**, 15019 (2000).
[35]C. G. Hemmingsson, N. T. Son, A. Ellison, J. Zhang, and E. Janzén, Phys. Rev. B **58**, R10119 (1998).
[36]C. G. Van de Walle, Phys. B: Phys. Condens. Matter **308**, 899 (2001).

RIGHTSLINK